*J Neurophysiol* 110: 1455–1467, 2013.
First published June 12, 2013; doi:10.1152/jn.00153.2013.



# Optogenetics through windows on the brain in the nonhuman primate

**Octavio Ruiz,[1]* Brian R. Lustig,[2]* Jonathan J. Nassi,[3]* Ali Cetin,[3] John H. Reynolds,[3] Thomas D. Albright,[1] Edward M. Callaway,[3] Gene R. Stoner,[1] and Anna W. Roe[2]**

[1]*Vision Center Laboratory, Salk Institute for Biological Studies, La Jolla, California;* [2]*Department of Psychology, Vanderbilt University, Nashville, Tennessee; and* [3]*Systems Neurobiology Laboratory, Salk Institute for Biological Studies, La Jolla, California*

Submitted 4 March 2013; accepted in final form 5 June 2013

**Ruiz O, Lustig BR, Nassi JJ, Cetin A, Reynolds JH, Albright TD, Callaway EM, Stoner GR, Roe AW.** Optogenetics through windows on the brain in the nonhuman primate. *J Neurophysiol* 110: 1455–1467, 2013. First published June 12, 2013; doi:10.1152/jn.00153.2013.— Optogenetics combines optics and genetics to control neuronal activity with cell-type specificity and millisecond temporal precision. Its use in model organisms such as rodents, *Drosophila*, and *Caenorhabditis elegans* is now well-established. However, application of this technology in nonhuman primates (NHPs) has been slow to develop. One key challenge has been the delivery of viruses and light to the brain through the thick dura mater of NHPs, which can only be penetrated with large-diameter devices that damage the brain. The opacity of the NHP dura prevents visualization of the underlying cortex, limiting the spatial precision of virus injections, electrophysiological recordings, and photostimulation. Here, we describe a new optogenetics approach in which the native dura is replaced with an optically transparent artificial dura. This artificial dura can be penetrated with fine glass micropipettes, enabling precisely targeted injections of virus into brain tissue with minimal damage to cortex. The expression of optogenetic agents can be monitored visually over time. Most critically, this optical window permits targeted, noninvasive photostimulation and concomitant measurements of neuronal activity via intrinsic signal imaging and electrophysiological recordings. We present results from both anesthetized-paralyzed (optical imaging) and awake-behaving NHPs (electrophysiology). The improvements over current methods made possible by the artificial dura should enable the widespread use of optogenetic tools in NHP research, a key step toward the development of therapies for neuropsychiatric and neurological diseases in humans.

primate optogenetics; artificial dura; optical imaging; in vivo epifluorescence; electrophysiology

TO UNDERSTAND THE NEURAL MECHANISMS that mediate perception and cognition in the human brain, we need to investigate species whose brains are, to the extent possible, homologous to those of humans and in animals capable of performing tasks that allow us to test cognitive functions that fail in these disorders. These considerations made nonhuman primates (NHPs) the model of choice for studying such neural mechanisms. Moreover, an understanding of the neural mechanisms underlying any sensorymotor or cognitive function requires not only recording electrophysiological activity during behavior, but also manipulating specific neural circuits and measuring the consequences.

The tools currently available to test causal relationships between neuronal activity and behavior in monkeys have major limitations. Cooling and pharmacological manipulations have poor spatial and temporal resolution; electrical stimulation has poor spatial resolution and creates electrical artifacts that interfere with neurophysiological recording. Moreover, none of these techniques have the capacity to target differentially specific neuronal subtypes.

Optogenetics uses molecular-recombinant techniques to make specific types of neurons responsive to light (Fenno et al. 2011), and it has excellent spatial and temporal resolution. Opsins expressed by neurons can be used to increase (Boyden et al. 2005) or silence (Chow et al. 2010) neuronal activity with millisecond temporal precision (Boyden et al. 2005; Han and Boyden 2007). For example, channelrhodopsin-2 (ChR2) and its variants (e.g., C1V1, ChETA, and SSFO) are light-sensitive cation channels used to depolarize neurons. Halorhodopsin (a light-activated chloride pump) and archaerhodopsin (a light-activated proton pump) are used to hyperpolarize neurons (Boyden et al. 2005; Han and Boyden 2007). Different combinations of viral vectors [e.g., adeno-associated virus (AAV) and lentivirus pseudotyped with vesicular stomatitis virus glycoprotein (VSV-G)] and gene promoters [e.g., $\alpha$-calcium/calmodulin-dependent protein kinase II (CaMKII$\alpha$)] bias opsin expression to either excitatory or inhibitory neurons (Dittgen et al. 2004; Han et al. 2009; Nathanson et al. 2009), and the targeting capacity of this approach will likely improve as new promoters are discovered. Optogenetics has been successfully used in rodents to study Parkinson's disease (Gradinaru et al. 2009; Kravitz et al. 2010), fear and anxiety (Ciocchi et al. 2010; Tye et al. 2011), and behavior (Huber et al. 2008; for review, see Bernstein and Boyden 2011).

Application of optogenetics to the NHP has been slow to develop. So far, only a few studies have used optogenetics to modulate neuronal activity in the NHP (Cavanaugh et al. 2012; Diester et al. 2011; Galvan et al. 2012; Gerits et al. 2012; Han et al. 2009, 2011; Jazayeri et al. 2012). Although these studies have demonstrated proof of principle, they have highlighted the fact that existing methods of virus and light delivery in the NHP are suboptimal. One of the key challenges involved is the thick and opaque primate dura mater, which necessitates the use of large-diameter devices that cause damage to the delicate brain circuitry under study. Here, we describe an approach in which a soft, transparent window replaces a section of the dura mater over the monkey brain. This optical window gives visual access to the underlying tissue for injection of viruses without cortical damage, permits in vivo tracking of opsin expression via epifluorescence imaging, and allows for highly precise targeting of recording electrodes and light delivery to sites of opsin expression. Moreover, the artificial dura (AD) allows optogenetics to be combined with intrinsic-imaging tech-

* O. Ruiz, B. R. Lustig, and J. J. Nassi contributed equally to this work.

Address for reprint requests and other correspondence: A. W. Roe, Dept. of Psychology, Vanderbilt Univ., 301 Wilson Hall, 111 21st Ave. S, Nashville, TN 37240 (e-mail: anna.roe@vanderbilt.edu).

niques. The approach thus provides a means of probing functional domains of the cortical map, measuring the effects of this stimulation across the cortical surface, and relating these changes to perception and behavior. Taken together, these capacities hold considerable promise for enhancing our understanding of cortical computation in the behaving primate.

## MATERIALS AND METHODS

### *Surgical Procedures*

Head posts, chambers, and AD were implanted using strictly aseptic surgical procedures. Monkeys were sedated with ketamine (10 mg/kg), anesthetized with isoflurane, and artificially ventilated. They were placed on a heating blanket, secured in a stereotaxic frame, and monitored continuously for end-tidal $CO_2$, heart rate, temperature, and respiratory function. All surgical procedures and experimental protocols were conducted in accordance with National Institutes of Health (NIH) guidelines and approved by the Animal Care and Use Committees of the Salk Institute and Vanderbilt University.

### *The Optical Window*

*Optogenetic recording chamber.* Chambers and chamber caps (Fig. 1*A*) were constructed from either Food and Drug Administration-approved nylon (Chen et al. 2002) or titanium. All chambers and caps were MRI-compatible. Chambers were implanted in a craniotomy (Fig. 1*A*) positioned over the cortical region of interest [primary visual cortex (V1) in the 3 monkeys reported in this study]. Figure 1*C* shows the titanium chamber. The 3 threaded holes serve to mount a removable stage that enables the use of microdrives for positioning electrodes and optical fibers over the cortex. All chambers had inner threading to fasten a screw cap to seal the chamber between recording sessions.

*The AD.* The key innovation of our approach is a durotomy into which a silicone AD is inserted. The custom-made AD is molded from silicone in the shape of a cylinder attached to a disk (Fig. 1*B*; Arieli et al. 2002; Chen et al. 2002). The flange, the part of the disk that extends beyond the cylinder like the brim of a hat, is inserted between the native dura and the cortex (Fig. 1*A*).

The placement of the AD flange beneath the native dura ensures that the durotomy cannot close beneath the AD; the cylindrical wall, inside the durotomy, prevents the native dura from growing into the chamber and over the window. The base of the hat within the cylindrical wall protects the cortex, serves as an optical window (Fig. 1*C*), and is penetrable by fine glass micropipettes, microelectrodes, and light.

*Chamber and AD implantation.* The chamber and AD are implanted using approaches developed for intrinsic imaging studies. Briefly, a trephine is used to create a circular craniotomy over the cortical area under study (~2-cm diameter). The exposed dura is cut and resected. The AD is then placed in the durotomy so that the flange lies under the edge of the native dura. The chamber is then secured to the bone around the AD (Fig. 1*A*). Two or more screws are placed in the skull, around the chamber, to serve as anchors for the cement. A thin layer of bone cement is applied between the bone and the rim of the chamber, and more cement is added, extending over the screws, to secure the chamber in position (Fig. 1, *A* and *C*). Chambers were made with minimal height to facilitate illumination during optical-imaging experiments and AD replacement. Chamber diameters were chosen based on the extent of cortex to be studied. The chambers used in this study had inner diameters between 17 and 21 mm; they were implanted near the occipital pole, over V1, and covered different proportions of V2 and V4 in each monkey. We have successfully implanted long-term optical chambers in rodents, squirrel monkeys, and macaque monkeys for use in optical-imaging experiments (e.g., Chen et al. 2005; Lu et al. 2010; Tanigawa et al. 2010). The present

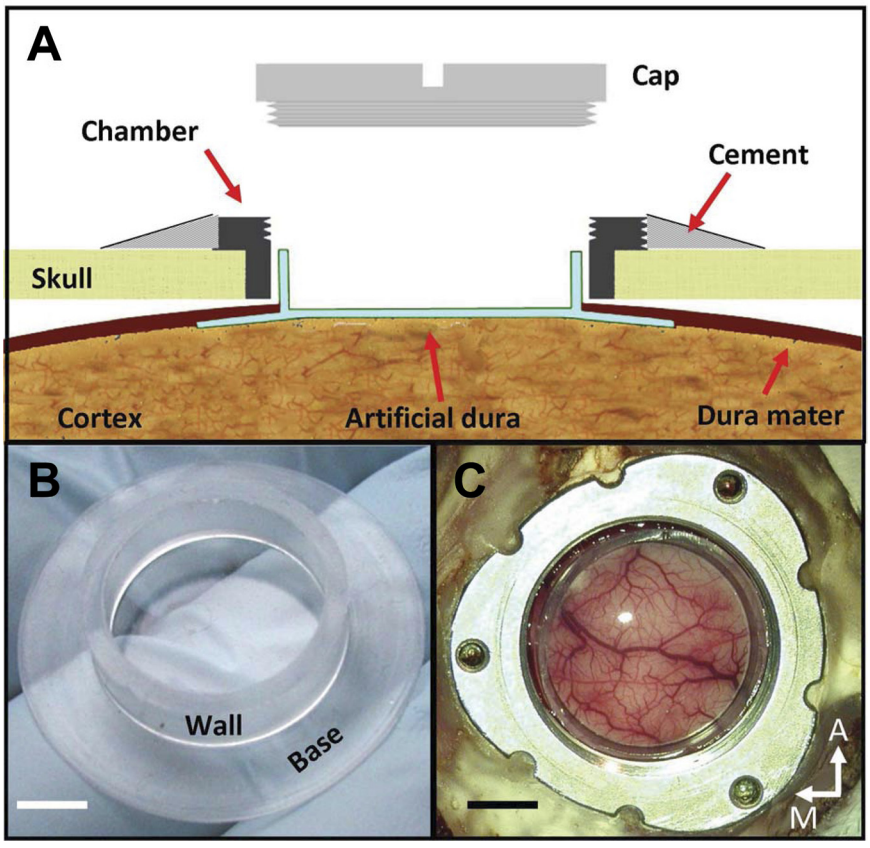


Fig. 1. Artificial-dura (AD) implant. *A*: schematic illustration of the implant, showing the relations between chamber, skull, native dura, AD, and cortex. The brim of the "hat," or flange, is inserted under the native dura and above the cortex. The AD window allows for a clear view of the cortical surface and provides access for imaging, injections, and electrode penetrations. *B*: optically clear silicone AD. This hat-shaped AD is composed of a cylindrical wall and a base. The area of the base surrounded by the wall is the window. *C*: view of macaque visual cortex through the optical chamber (*monkey C*). M, medial; A, anterior. Scale bars: 5 mm.

work reports the use of our AD in macaque monkeys for optogenetic experiments.

*Chamber maintenance.* Proper maintenance of the AD is essential to avoid infection and to prevent excessive tissue growth between the wall of the AD and the chamber. The chamber should be cleaned at least twice each week. The chamber is only opened under aseptic conditions. First, the exterior of the chamber is cleaned and carefully wiped with aseptic solutions such as Nolvasan and Betadyne. The cap is then removed, and any fluids within the chamber are absorbed with sterile gauze. The top edge of the chamber is wiped with hydrogen peroxide and dried. The interior of the chamber is rinsed with sterile saline, and saline is immediately absorbed with gauze so as not to permit fluid continuity between the interior and the exterior of the chamber. There is typically some tissue growth, from the edge of the craniotomy, which invades the space between the chamber wall and the silicone cylinder. This gelatinous tissue is removed by wiping it with cotton-tipped swabs. Removal of this tissue must be done regularly (at least once per week) to prevent further maturation into membranous tissue. Before closing the chamber, a small piece of gauze with approximately 0.05–0.1 ml of antibiotic (e.g., amikacin or gentamicin) is placed within the chamber, over the AD window. Additionally, a silicone plug is placed over the gauze to fill the empty space between the AD and the cap and to prevent the AD from popping out from the durotomy. Cefazolin should not be used as antibiotic, as it can induce seizures. A sterile chamber cap is then put in place, and the space between the chamber and the cap is sealed with melted bone wax to prevent entry of bacteria.

### *Viral Preparation and Injections*

In the present study, two different types of viruses were used (VSV-G-pseudotyped lentivirus and AAV5), carrying constructs that encoded one of three opsins [ChR2, archaerhodopsin-T inhibitory opsin (ArchT), or C1V1], fused to one of three fluorescent reporter proteins [enhanced yellow fluorescent protein (EYFP), green fluorescent protein (GFP), or mCherry (a red fluorescent protein, RFP)]. In all cases, expression was driven by the promoter CaMKII$\alpha$ (Dittgen et al. 2004). The titers of all lentiviruses used were between $0.4 \times 10^{10}$ and $3 \times 10^{10}$ transducing units per milliliter (TU/ml). The titer of the AAV5 was $2.0 \times 10^{12}$ TU/ml. Table 1 lists the viral constructs used, their source, and the tests performed with each virus. CaMKII$\alpha$-ChR2-mCherry, CaMKII$\alpha$-ArchT-GFP, and CaMKII$\alpha$-ChR2-EYFP lentiviruses were produced by the Salk Institute viral vector core using constructs provided by Dr. Karl Deisseroth (Chr2-mCherry and ChR2-EYFP) or Dr. Ed S. Boyden (ArchT-GFP). The AAV5-CaMKII$\alpha$-C1V1-EYFP virus was a gift from Dr. Deisseroth. The CaMKII$\alpha$-C1V1-EYFP lentivirus was produced by A. Cetin using a construct provided by Dr. Deisseroth. All lentiviruses were pseudotyped with VSV-G.

Viral injections were made under isoflurane anesthesia using glass pipettes [cat. no. 1B120F-4; World Precision Instruments (WPI)] with tips pulled to a diameter of approximately 30–40 $\mu$m. We found this diameter to be a good compromise between two factors. *1*) Pipettes with thinner tips cause less cortical damage but bend and break when trying to penetrate the AD; they are also more difficult to fill with virus and get easily clogged. *2*) Pipettes with larger-diameter tips are sturdy but allow silicone to enter the pipette, potentially clogging the tip and compromising the sealing properties of the AD. A stereotaxic micromanipulator was used to insert pipettes into the cortex either through the exposed pia mater during the initial implant surgery or, subsequently, through the AD. Care was taken to avoid surface vessels by viewing through a microscope during pipette insertion. We used slightly different parameters for the different injections and monkeys. For *monkeys M* and *C*, clusters of two to five injections were made. In each pipette penetration, we injected ~0.5 $\mu$l of virus, slowly, over approximately 10–20 min at each of three depths (1.2, 0.8, and 0.4 mm) using a picospritzer (model PV820; WPI; 8- to 20-ms pulses of approximately 20–25 psi delivered at approximately 0.2–0.6 Hz). An entire site was completed in 45 min. In *monkey A*, we injected every 200 $\mu$m in each penetration, spanning the entire thickness of cortex (~2 mm), with a duration of approximately 1–2 min per depth. For the AAV5-C1V1 site, we made two penetrations; for the Lenti-C1V1 site, one penetration. In all cases and monkeys, we injected ~0.5 $\mu$l per depth.

### *Histology*

*Monkey M* was given an overdose of anesthetic (100 mg/kg pentobarbital) and perfused transcardially with fixative (4% paraformaldehyde). Before sectioning, the ability to detect fluorescence from opsin- and fluorophore-expressing neurons through the brain surface was assessed. We used commercial "miner-lamp" goggles that incorporate wavelength-specific illumination with the appropriate emission filters for the fluorescent reporter proteins used in this study (BLS, Budapest, Hungary). For microscopy, parasagittal sections were cut at 50-$\mu$m thickness, using a freezing microtome. A series of every eighth section was mounted and coverslipped for analysis of native fluorescence using an epifluorescence microscope and digital image-capture software.

### *Optical Imaging*

Optical imaging was conducted in multiple sessions in anesthetized (1–2 $mg \cdot kg^{-1} \cdot h^{-1}$ Pentothal) and paralyzed (100 $\mu g \cdot kg^{-1} \cdot h^{-1}$ Norcuron) *monkey M*. Images of cortical-reflectance change were acquired, using 630-nm illumination, by an Imager 3001 system (Optical Imaging, Germantown, NY). For detailed imaging methods, see

Table 1. *Optogenetic agents and tests reported in this study*

| Viral Vector | Promoter, Opsin, and Fluorescent Marker | Source and Preparation | Opsin Action | Purpose in This Study (*Monkey* - Experiment) |
|---|---|---|---|---|
| Lenti | CaMKII$\alpha$-ChR2-mCherry | D, C, S | Depolarize | *M* - Optical imaging |
| Lenti | CaMKII$\alpha$-ArchT-GFP | B, C, S | Hyperpolarize | *M* - Histology<br>*C* - In vivo epifluorescence |
| Lenti | CaMKII$\alpha$-ChR2-EYFP | D, C, S | Depolarize | *C* - In vivo epifluorescence<br>*C* - Electrophysiology |
| AAV5 | CaMKII$\alpha$-C1V1 (E122T/E162T)-EYFP | D | Depolarize | *A* - Electrophysiology<br>*A* - In vivo epifluorescence |
| Lenti | CaMKII$\alpha$-C1V1 (E162T)-EYFP | D, C | Depolarize | *A* - Electrophysiology<br>*A* - In vivo epifluorescence |

Lenti, lentivirus; AAV5, adeno-associated virus serotype 5; CaMKII$\alpha$, $\alpha$-calcium/calmodulin-dependent protein kinase II; ChR2, channelrhodopsin-2; mCherry, a red fluorescent protein; ArchT, archaerhodopsin-T inhibitory opsin; GFP, green fluorescent protein; EYFP, enhanced yellow fluorescent protein; C1V1, ChR2 variant; B, Boyden laboratory, Massachusetts Institute of Technology; C, A. Cetin and E. M. Callaway, Salk Institute; D, Deisseroth laboratory, Stanford University; S, Salk Institute viral vector core.

Chen et al. (2008), Lu et al. (2010), and Tanigawa et al. (2010). Image acquisition (4 frames per second) included 2 frames before visual stimulus as baseline and 14 frames during stimulus presentation. The monkey's eyes were fitted with contact lenses to focus on a computer monitor. Visual stimuli were full-field achromatic gratings, presented to 1 eye or the other, using electromechanical shutters placed in front of each eye. All conditions were pseudorandomly interleaved and repeated ≥30 times. Optogenetic experiments included 4 frames before photostimulation as baseline, 3 frames during photostimulation, and 13 frames to assess the cortical response.

### *Brain-Surface Fluorescence*

Two commercial miner-lamp goggles (BLS) were used to monitor fluorescence in vivo on the brain surface, associated with virus injection sites. One pair of goggles had a blue excitation light and GFP/YFP emission filters. The other pair of goggles was used to check for nonspecific fluorescence; it had a green excitation light and RFP emission filters. Photographs were taken with a conventional point-and-shoot digital camera using apertures from *f*/2 to *f*/5.6, exposure times ¼ to 1 s (sensitivity = 400 ISO or more, manual operation), placing its lens directly over the ocular of a dissection microscope aimed toward the chamber. The goggles were positioned between the microscope and the chamber, with one filter in contact with and covering the microscope objective. The lamp of the goggles was aimed toward the chamber. It is important to have the filter of the goggles perpendicular to the optical axis of the microscope because filter angle affects the transmitted spectrum. Better results should be obtained with a higher signal-to-noise image sensor and dedicated filters and illuminators.

### *Photostimulation Devices*

We used two different illumination systems. To activate ChR2 in *monkeys A* and *M*, we used a house-made blue light-emitting diode (LED; Osram LB W5AP-JYKY-35) coupled directly to a 1- or 2-mm diameter optical fiber. We used a green laser as a control for ChR2 activation specificity in the optical imaging experiments (532 nm, 100 mW). To activate C1V1 in *monkey A*, we used a green laser (532 nm, 300 mW; OEM Laser Systems) that passed through several optical elements, including neutral density filters and a beam sampler, before being coupled to a 600-$\mu$m diameter multimode optical fiber (Thorlabs).

### *AD Stabilization*

The AD is softer and more elastic than the native dura and thus does not dampen the brain movements associated with respiration as much as the native dura. To dampen those movements, we used transparent, rigid-plastic stabilizers during virus injections, optical imaging, and electrophysiological recordings. Although we used different versions of these stabilizers in different experiments, the simplest version was a disk with three "legs," which extended from the disk and were bent upward when placed into the chamber. The disk had one or more holes cut in it to allow the passage of pipettes or electrodes through the AD and into the brain. The disk was lowered inside the AD wall until it sat directly on the AD window. The three legs press against the AD wall along their length and become secured by their ends "clicking" into the threading of the chamber as the stabilizer is pushed into the chamber. The stabilizer applies a small amount of mechanical pressure to the AD window, thereby reducing brain movements.

### *Electrophysiology*

We used thin epoxy-coated tungsten electrodes (75-$\mu$m shank diameter; FHC) or glass-coated tungsten electrodes (250-$\mu$m shank diameter; Alpha Omega). Stimulus presentation and data collection were controlled by custom-written programs. Electrophysiological signals were amplified and stored for offline analysis. We machined special adapters for the optical chambers to position electrodes and optical fibers.

## RESULTS

### *Health and Stability of Cortex Over Time*

Three rhesus macaques were used in this study. ADs and chambers were implanted over the V1 of each monkey (Fig. 1). Optical-imaging data were collected in one anesthetized monkey (*M*), and electrophysiological data were collected in two alert monkeys (*C* and *A*). In all three monkeys, the optical window provided a stable long-term preparation: the AD remained optically clear, vessels were identifiable, and cortex was healthy for the duration of this study (~1 yr). Figure 2, *A* and *B*, shows the AD chamber of *monkey A* 1 wk and ~6 mo after implantation, respectively. With regular maintenance, the chamber remained infection-free. Over a span of months, a layer of neomembrane appeared beneath the window, compromising visualization and access to the underlying cortex (Fig. 2*B*, *left*). As the neomembrane thickens, penetrating with thin electrodes becomes difficult, and the AD itself becomes less secure. The neomembrane was surgically removed under anesthesia, restoring optical clarity and access to the cortex (Fig. 2*B*, *right*). The procedure to remove the neomembrane is similar to a durotomy, with special care needed due to possible adhesions and vessels that can join the neomembrane to the cortex. As seen in Fig. 2*B*, *right*, the cortex and vessels under the AD were healthy 6 mo after the initial AD implant. In all of our monkeys, some vessels changed size, but their locations remained stable, and it was easy to identify matching vessels weeks and months apart. New fine vessels appeared within the neomembrane that slowly grows above the cortex (compare, for example, the chamber top-right quadrant in Fig. 2, *A* and *B*, *right*); this neovasculature was readily distinguished from cortical vessels as it is at a different plane of focus when viewed under a microscope. These vessels do not interfere with optical imaging or photoelectrophysiological experiments.

As we have previously shown (Lu et al. 2010; Tanigawa et al. 2010), stable optical images of functional organization can be obtained over time. To illustrate, Fig. 2, *C* and *D*, shows two ocular-dominance maps in V1 of *monkey M* taken >3 mo apart. These maps reveal columns of left-eye (dark stripes) vs. right-eye (clear stripes) responses. The ocular-dominance columns exhibit the same general size and arrangement 3 mo apart. Compare, in particular, the region within white boxes in Fig. 2, *C* and *D*: the two boxes were drawn using the vasculature as reference, resulting in near-indistinguishable ocular-dominance maps framed by each box. Note that several virus injections were made over this 3-mo period (across different sessions), demonstrating that neither the viral injections nor the expression of the optogenetic constructs affected the health of the cortex or the integrity of functional domains.

In summary, the stability of functional maps over time suggests that our approach is appropriate for long-term studies compatible with repeated imaging, electrophysiology, and optogenetic manipulations.

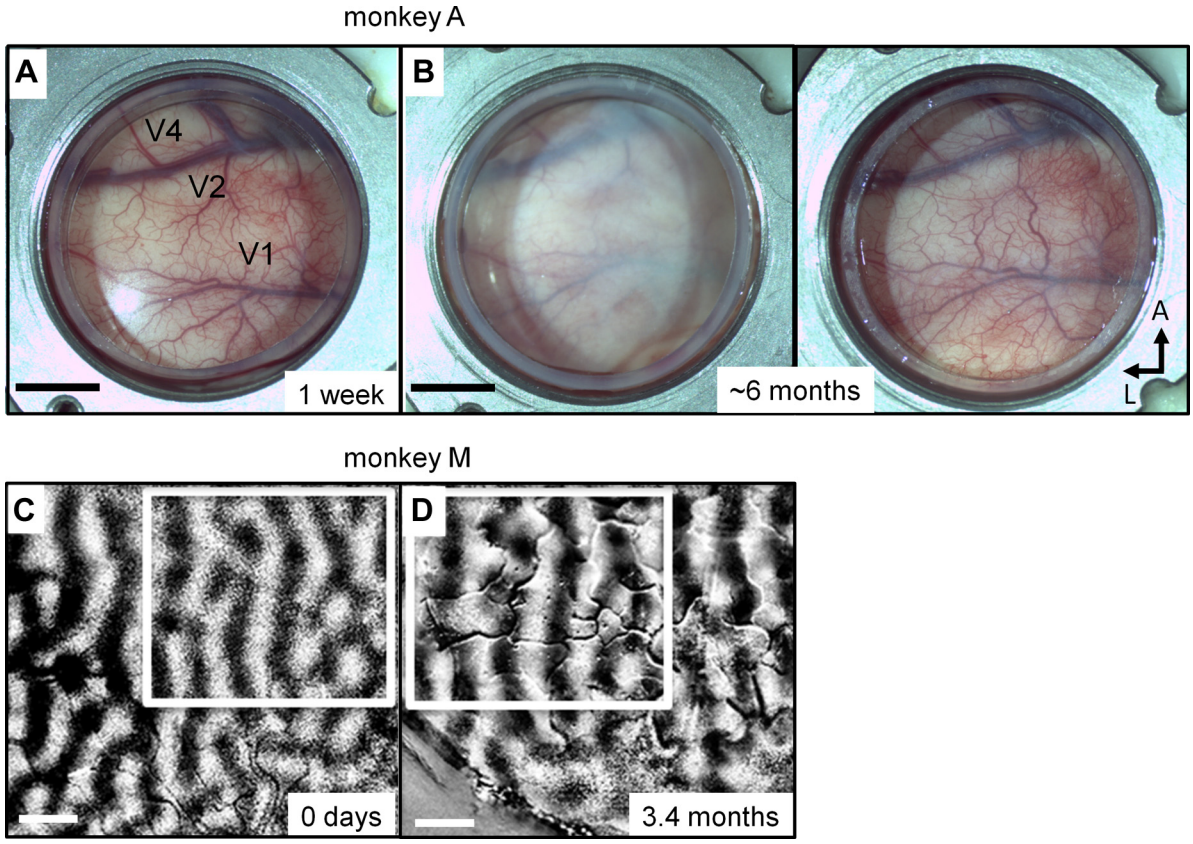


Fig. 2. Long-term cortical health. *A* and *B*: view of cortex in *monkey A* through the optical window 1 wk (*A*) and ~6 mo (*B*) following chamber implant. Over the course of months, a neomembrane grows underneath the AD, compromising visualization and access to the underlying cortex (*B*, *left*). The neomembrane can be removed during an anesthetized procedure, restoring optical clarity and access (*B*, *right*). Approximate locations of V1, V2, and V4 are indicated in *A*. Scale bars: 5 mm. L, lateral. *C* and *D*: ocular-dominance maps, measured with optical imaging, in a different monkey (*monkey M*) on *day 0*, just before AD and chamber implant (*C*), and 104 days after implantation (*D*). Ocular-dominance maps are unaltered by the presence of the AD (*D*) and were stable not only after hundreds of days, but also after several virus injections in cortex (see text for details). Boxed areas indicate corresponding regions within the 2 fields of view, aligned according to the vessel maps; notice the stability of the ocular-dominance domains measured >3 mo apart. Scale bars: 1 mm.

*Window for Targeted Viral Injections*

The AD allows for precisely targeted and minimally invasive injections of viral vectors using fine pulled-glass micropipettes. Accurate targeting is enabled by reference to anatomic landmarks such as cortical sulci, microvasculature patterns, and functional maps obtained with optical imaging. Viral injections can be targeted, for example, into orientation domains or ocular-dominance columns mapped with optical imaging.

Figure 3*A* shows a virus-filled micropipette (~40-$\mu$m tip diameter) during a viral-vector injection in *monkey M* performed under anesthesia to minimize movement. The pipette was inserted slowly via a micromanipulator. Brain pulsations were reduced with a rigid plastic stabilizer placed against the AD (see *AD Stabilization* in MATERIALS AND METHODS). A hole in the stabilizer allowed passage of a pipette through the AD. We paid attention to avoid surface vessels; this is critical as bleeding increases light absorption and scattering. The small size of the pipette tip, cortex stabilization, and vessel avoidance prevent tissue damage and markedly increase the likelihood of successful long-term optogenetic studies.

We injected viral vectors through the AD of *monkey M* in three different sessions. As lentivirus has limited spread in the cortex (Dittgen et al. 2004; Nathanson et al. 2009), injections were made in clusters of two to five penetrations, ~300 $\mu$m apart, to create large and dense regions of expression (Fig. 3*B*). For each penetration, virus was injected at three depths: 1.2, 0.8, and 0.4 mm from the brain surface. We used low-pressure injections (approximately 20–25 psi) to minimize tissue damage and prevent virus refluxing back up the injection site. Our ability to visualize vessel patterns allowed us to target the injections in these clusters across sessions accurately (for example, *cluster 1* was produced in 3 sessions, each session 1–2 wk apart). Each red dot indicates a pipette penetration that injected lentivirus carrying the CaMKII$\alpha$ promoter and genes for ChR2 fused to the fluorophore mCherry (Lenti-CaMKII$\alpha$-ChR2-mCherry). Green dots show the injection sites for a similar lentivirus that carried genes for ArchT fused to the fluorophore GFP (Lenti-CaMKII$\alpha$-ArchT-GFP). These viruses were injected into specific functionally identified ocular-dominance columns revealed by optical imaging (Fig. 3*C*): Lenti-ChR2 injections (red dots) were made in right-eye columns (white zones); Lenti-ArchT injections (green dots) were targeted into left-eye columns (gray zones). The cortex remained in excellent health following these multiple injections and recording sessions. We have never had any case of a pipette breaking during injections through the AD. All of our injections were made in anesthetized (not paralyzed) monkeys with

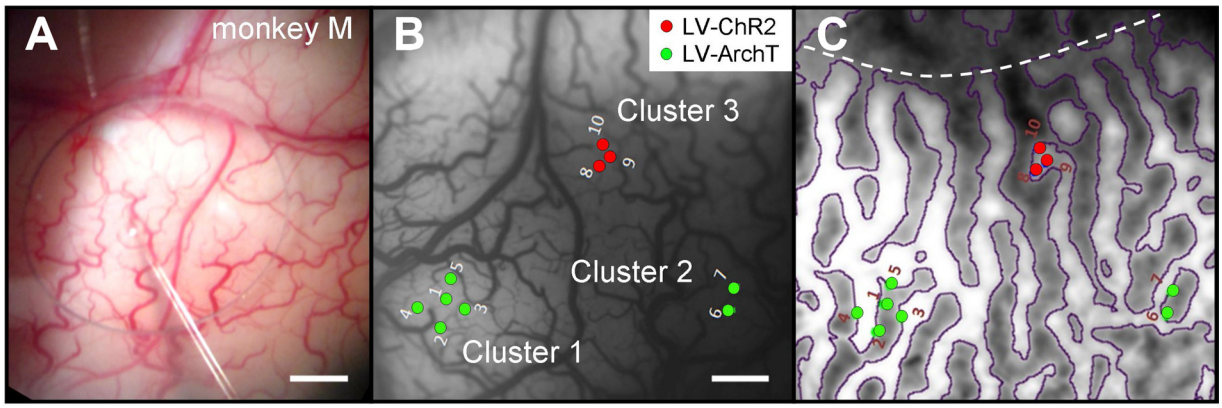


Fig. 3. Targeted injections of optogenetic viral vectors. *A*: micropipette inserted through AD under anesthesia (*monkey M*). Circular opening is a hole in a cortical stabilizer placed on top of AD. *B*: location of virus injections in V1 of *monkey M* superimposed on a blood-vessel map (image acquired during an optical imaging session). Green dots indicate Lenti-ArchT injections (LV-ArchT), grouped in 2 separate clusters (*1* and *2*). Red dots represent Lenti-ChR2 (LV-ChR2) injections, in *cluster 3*. These injections were done in different sessions. For example, *cluster 1* was made in 3 sessions; *penetrations 1–3* were made the day of the AD and chamber implantation; *penetration 4* was made in a different session, 8 days later; and *penetration 5*, 14 days later. *C*: ocular-dominance map (same field of view as in *B*) obtained with optical imaging. Dotted line: V1/V2 border. The Lenti-ChR2 injections (*cluster 3*, red dots) were made in a right-eye column (lighter stripes); Lenti-ArchT injections (*clusters 1* and *2*, green dots) were made predominantly in left-eye columns (darker stripes). Scale bars: 1 mm.

heads held in a stereotax. A question for future experiments is whether injections with glass pipettes can be made in awake monkeys with fixed heads. If so, this would remove the potential of encountering complications associated with anesthesia and surgical procedures.

### *Detection of Viral Expression*

One difficulty in NHP optogenetics is the inability to visualize expression of fluorescent reporter genes in vivo through the native dura. Thus successful viral expression is usually confirmed by epifluorescence microscopy carried out on postmortem tissue. Recently, a method has been developed to assess fluorescence intensity levels in vivo using a sophisticated optical arrangement that measures fluorescence through the same optical fiber used for photostimulation (Diester et al. 2011). This is an important tool enabling detection of viral expression at the injection site. However, the size of the device and the invasiveness of the technique have the potential to cause significant tissue damage. Conversely, the AD approach provides a noninvasive means of assessing viral expression.

### *Postmortem Epifluorescence Imaging: Monkey M*

We first determined whether we could visualize optogenetic fluorescently tagged opsins through the surface of a fixed brain. Figure 4*A* shows the occipital pole of *monkey M*'s brain fixed for histology (paraformaldehyde) after having allowed sufficient time for the opsins to express. Figure 4*B* shows a photograph of the same brain region taken through commercial YFP/GFP miner-lamp goggles (blue-excitation/green-emission filters). Two fluorescent spots are evident in the picture at locations corresponding to Lenti-ArchT-GFP *clusters 1* and *2* in Fig. 3*B*. Histological analysis of cut sections, using epifluorescence microscopy, revealed neurons expressing GFP at these two cortical locations (data not shown).

### *In Vivo Epifluorescence Imaging: Monkeys C and A*

Figure 4*C* shows *monkey C*'s chamber under natural light, and Fig. 4*D* shows the chamber viewed through GFP/YFP goggles during a session 7 days after Lenti-CaMKII$\alpha$-ArchT-GFP injections and 23 days after Lenti-CaMKII$\alpha$-ChR2-EYFP injections. Two fluorescent spots, which match the location of the respective virus injection sites, are clearly visible in cortex through the AD. Observations through RFP goggles showed that a small proportion of this fluorescence was not specific (data not shown). This nonspecific fluorescence decreased rapidly and was no longer present ~2 mo after the virus injections, leaving only the green/yellow fluorescence associated with the opsin-fluorophore pair.

Similar results were obtained in *monkey A*, injected with AAV5 and lentivirus, both carrying a C1V1-EYFP construct (Fig. 4, *E* and *F*). In this monkey, we detected fluorescence through the optical window at the injection sites a few days after the AAV5-CaMKII$\alpha$-C1V1-EYFP injections; fluorescence at the site of the Lenti-CaMKII$\alpha$-C1V1-EYFP injection was apparent ~3 wk after injection. The fluorescence observed at the injection sites in *monkey A* was clearly distinguished from autofluorescence (or other nonspecific sources of fluorescence) by observation through RFP goggles, which did not reveal a detectable signal (data not shown).

Fluorescence was observed every time we used the goggles to check for expression over a time span of 3 (*monkey C*) and 9 (*monkey A*) mo. The intensity of fluorescence tended to decrease with time but did not disappear. The most likely cause for this decrease is the growth of neomembrane between the cortex and the AD, which gradually thickens and eventually becomes opaque. This interpretation is supported by the observation that the intensity of fluorescence increased on removal of the neomembrane and replacement of the AD. Photobleaching during imaging could also have contributed to the diminished intensity of fluorescence. Imaging with the goggles was, however, brief and infrequent. Moreover, opsin-fluorophore proteins should have been continuously expressed by infected neurons so we believe the photobleaching was not a major contributor.

Noninvasive in vivo epifluorescence imaging thus provides an important tool in optogenetic experiments both by confirm-

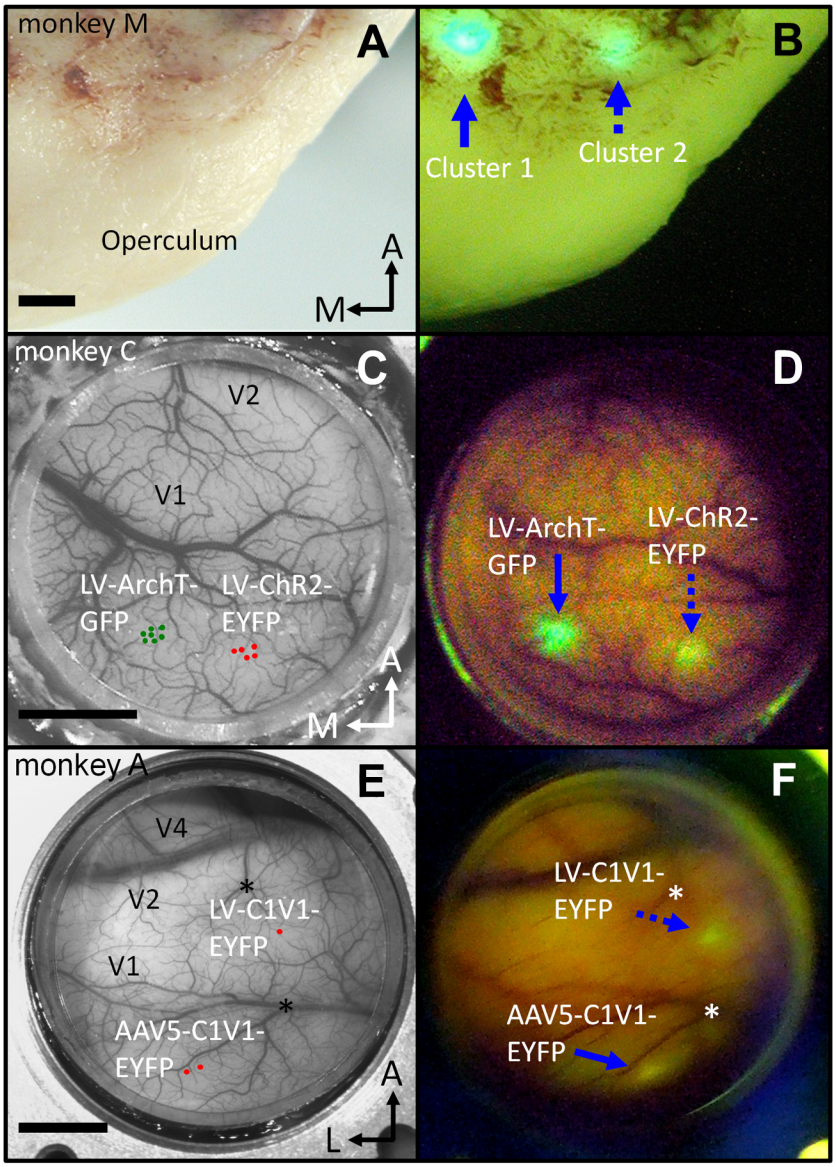


Fig. 4. Epifluorescence imaging of optogenetic agents, seen through the surface of the brain. *A* and *B*: paraformaldehyde-fixed brain of *monkey M*, 6 mo after Lenti-ArchT-GFP injections. *A*: operculum of the right hemisphere. *B*: same view as *A*, seen through commercial "miner-lamp" goggles (blue-excitation/green-emission filters). The 2 fluorescent spots (blue arrows) colocate with the 2 Lenti-ArchT-GFP injection clusters (compare with Fig. 3*B*; *clusters 1* and *2*). *C* and *D*: epifluorescence imaging in vivo, *monkey C*. *C*: image of cortical vasculature through the AD of *monkey C* with superimposed virus injection locations. *D*: image showing fluorescent-reporter protein expression at the 2 spots matching the injection sites indicated in *C*. Photograph *D* was taken 7 days after the Lenti-CaMKIIα-ArchT-GFP injections (blue arrow) and 23 days after the Lenti-CaMKIIα-ChR2-EYFP injections (dotted blue arrow). *E* and *F*: virus-injection sites and epifluorescence imaging in *monkey A* (same description as *C* and *D*). Photographs *E* and *F* were taken from a slightly different perspective, making the adeno-associated virus (AAV) site appear closer to the right border of the chamber in *F*. Asterisks in *E* and *F* mark conspicuous vessel branch points for reference. Blue arrow in *F*: site of AAV5-CaMKIIα-C1V1-EYFP injection. Dotted blue arrow: site of Lenti-CaMKIIα-C1V1-EYFP injection. Photograph *F* was taken 31 days after injections. Epifluorescence images (*B*, *D*, and *F*) are single-exposure photographs taken as described in MATERIALS AND METHODS. Scale bars: 2 mm (*A* and *B*) and 5 mm (*C*–*F*).

ing protein expression and by guiding targeting of light and recording electrodes to opsin-expressing sites.

### *Effects of Photostimulation*

We used two methods to assess the success of the optogenetic transfection: intrinsic-signal optical imaging and extracellular single-unit electrophysiology.

### *Intrinsic Signal Optical Imaging*

When visual cortical neurons are activated by visual stimuli, this activity is accompanied by hemodynamic changes in cortex due to stimulus-induced deoxygenation events. Such events are detectable as a darkening of the blood and cortical tissue and can be optically detected as a negative reflectance change commonly referred to as the intrinsic signal. Cortical intrinsic signals are on the order of 0.1% in magnitude and typically peak around 2–3 s poststimulus onset (Grinvald et al. 1986, 1991). If neurons express optogenetic proteins, then wavelength-specific photostimulation of those neurons should induce neuronal activity and an accompanying local negative reflectance change.

Sixty-five days after virus injection, we located the ChR2 cluster of *monkey M* using vasculature as a guide. We positioned a 1-mm diameter optical fiber over the ChR2 cluster (Fig. 3*B*) and coupled the other end of the fiber to either a blue LED (470 nm) or a green laser (532 nm). The irradiances measured at the cortical end of the fiber were 20 mW/mm$^2$ (blue LED) and 40 mW/mm$^2$ (green laser). Optical-imaging frames were collected (4 Hz, 250 ms per frame, 5 s per trial) during optical stimulation of the cortex with the fiber optic.

As shown in Fig. 5*A*, baseline reflectance was measured for 4 frames (*top* row of Fig. 5*A*, fiber tip visible at left side of frame), followed by photostimulation through the fiber (*frames 5–7*). The blue light (pulses lasting 600 ms, pulse width = 20 ms, 24 Hz) saturated the optical imaging system during *frames 5–7*. Immediately following the photostimulation offset, a focal darkening appeared in the cortex (*frame 8*). This signal (darkening) persisted over the next 3 s (*frames 9–20*). Figure 5*B* shows, magnified, 2 frames in the sequence: 1 before (4th

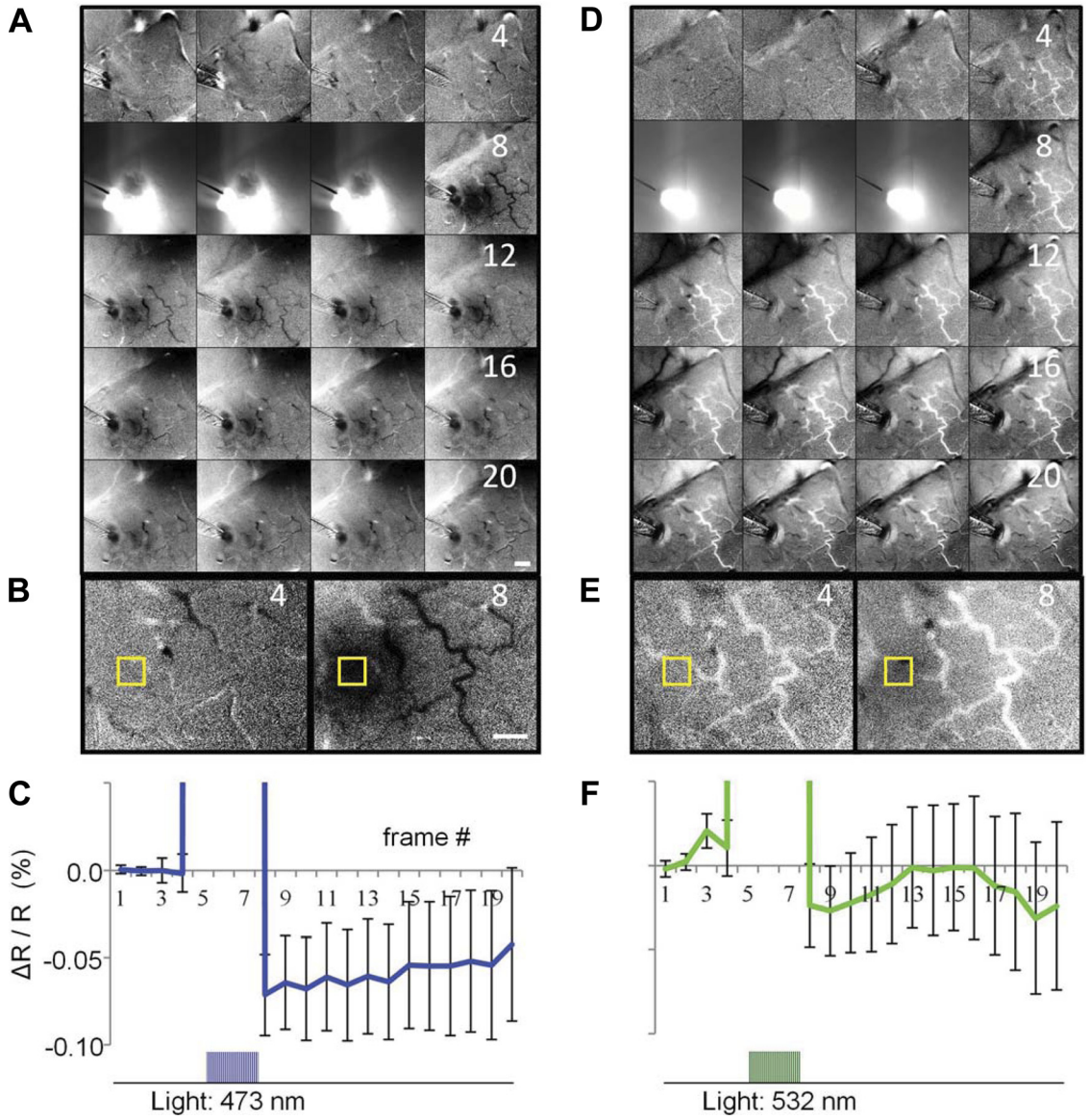


Fig. 5. Intrinsic-signal optical imaging of cortex, through the AD, during an optogenetic-activation experiment in *monkey M*. *A*: 16 frames (250 ms per frame) of the optical-imaging acquisition. The 1st 4 frames (*1–4*; *top* row) were captured before photostimulation, the next 3 frames (*5–7*) during photostimulation, and the rest (*8–20*) after the photostimulation was turned off. Each image is blank- and 1st-frame subtracted. Blue light pulses (train duration = 600 ms, pulse duration = 20 ms, 24 Hz; 470 nm, 20 mW/mm$^2$) were directed to the ChR2 site via a 1-mm diameter optical fiber placed over the AD. The fiber tip can be seen by the left border of the 1st frame in *A*. *B*: enlarged view of *frames 4* and *8*. Yellow box represents the region of interest (ROI) selected to calculate the time course of the optical signal at the photoactivated ChR2 site. Scale bars: 1 mm. *C*: time course of the reflectance change (ΔR/R) at the photostimulation site. There is a significant negative reflectance change of ~0.1% associated with the photostimulation consistent with the time course and magnitude of intrinsic signals (*t*-test for *frames 8*, *9*, and *10* for blue laser vs. blank condition, $P = 0.0082$, 0.0294, and 0.0344, respectively). Photostimulation artifact in *frames 5–7* is off scale. Error bars: standard error of the mean. *D–F*: control data, same conventions as in *A–C*: green light (523 nm, 40 mW/mm$^2$; same temporal pattern as blue light). *D*: green light did not elicit a significant reflectance change in the ChR2 site: notice absence of darkening in cortex in the region illuminated by the optical fiber (*frames 8–20*). *E*: enlarged view of *frames 4* and *8* that shows minimal or no reflectance change associated with the green light. *F*: time course of the signal in ROI; the signal does not deviate significantly from baseline (*t*-test for *frames 8*, *9*, and *10* for green laser vs. blank condition, $P = 0.3865$, 0.3678, and 0.4726, respectively). The 600-ms photostimulation train (applied during *frames 5–7*) is indicated at the *bottom* of *C* and *F*. All images are the sum of 40 trials.

frame) and the other following (8th frame) the photostimulation period.

The time course of the reflectance change in the focally activated area (sampled from yellow box in Fig. 5*B*) is plotted in Fig. 5*C*. The baseline reflectance (1st 4 frames) is followed by saturating photostimulation (3 frames off scale). This artifact is followed by a ~0.1% negative reflectance change that slowly returns toward baseline, consistent with the intrinsic optical-image signal that typically follows neuronal activation.

To confirm that the observed changes in reflectance were not due to heat or other nonspecific effects of illumination (Cayce et al. 2011; Christie et al. 2012), we switched the light source to a green laser (much less efficient in activating ChR2) while maintaining the fiber position over the ChR2 site. As shown in Fig. 5, *D–F*, green light produced no significant change in reflectance from baseline (compare *frames 8–20* in Fig. 5, *A* and *D* and *frames 4* and *8* shown enlarged in Fig. 5*E*). The lack of an intrinsic signal elicited

by green light is further confirmed by the time course of the reflectance (Fig. 5*F*), which does not deviate significantly from baseline after photostimulation (*frames 8–20*). Thus the green laser, despite having a higher irradiance than the blue light (40 vs. 20 mW/mm$^2$, respectively), produced no significant intrinsic-signal response in the ChR2 cluster. The response was wavelength-specific, consistent with the absorption spectrum of the ChR2 opsin, and hence was not due to nonspecific effects of light on the tissue.

In conclusion, the wavelength-specific induction of intrinsic signal suggests that neurons at the ChR2 injection site expressed the opsin and were appropriately activated by photostimulation. Moreover, we have demonstrated that photo-elicited activity can be monitored via intrinsic-signal optical imaging. This combination of optical window, optical imaging, optogenetics, and external photostimulation provides a noninvasive, all-optical activation and readout assessment of cortical activity.

### *Electrophysiology*

We recorded single-neuron activity elicited by photostimulation in V1 of *monkeys C* and *A* (Fig. 6, *A* and *B*). In all of these experiments, illumination was directed at the cortical surface via an optical fiber placed above the AD. Figure 6*A* shows an optical fiber and an electrode aimed at the ChR2 cluster of *monkey C*'s brain (Fig. 4, *C* and *D*). This experiment was conducted 3 mo after virus injections. The photograph also

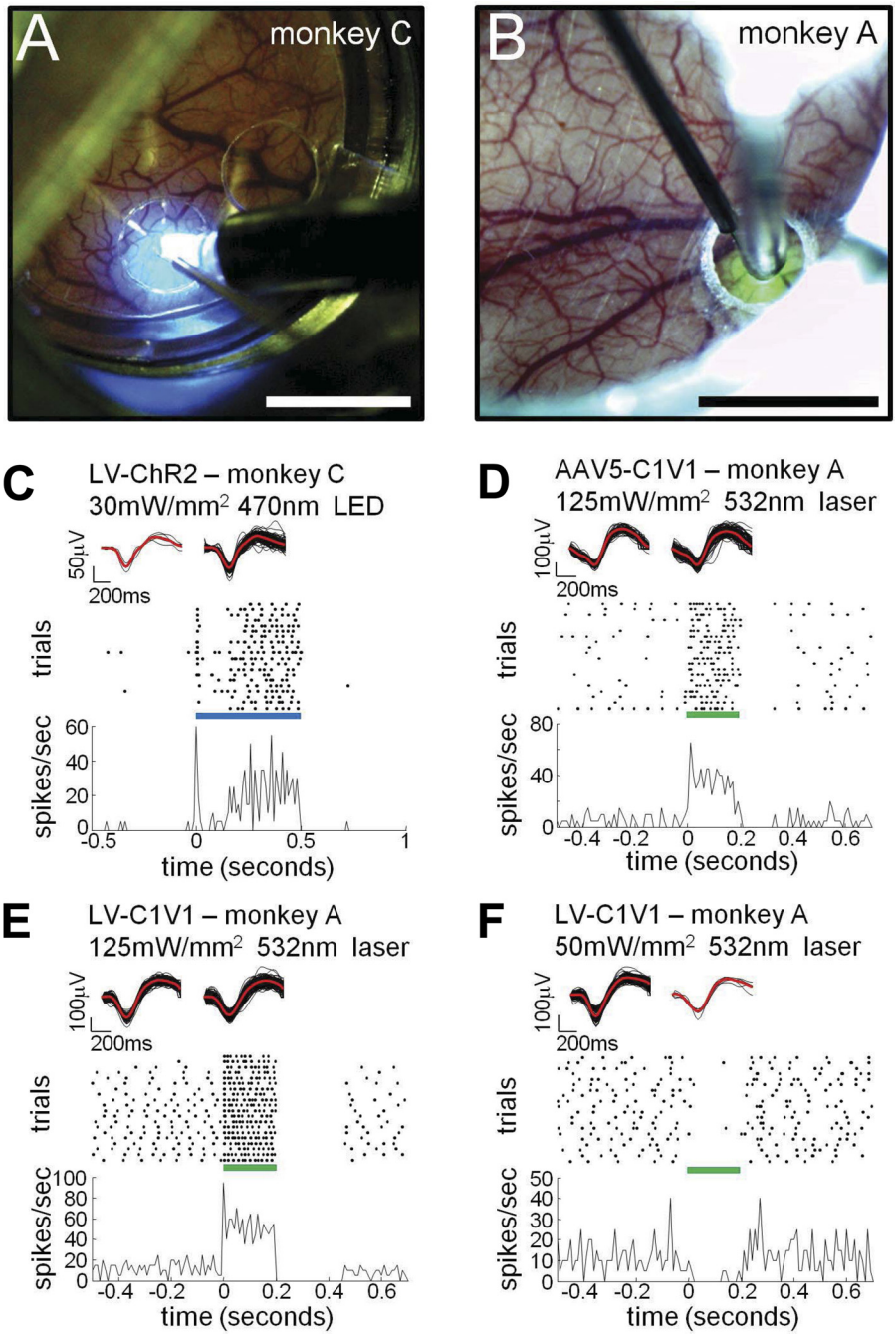


Fig. 6. "Photoelectrophysiology" of V1 neurons in 2 alert monkeys through the AD. *A*: optical-fiber and electrode arrangement at ChR2 site in *monkey C*. *B*: arrangement for neuronal recording of C1V1 site in *monkey A*. Scale bars: 5 mm. *C*: extracellular single-unit recording at the Lenti-ChR2 site in *monkey C* in response to a 500-ms photostimulation pulse of blue light from a light-emitting diode (LED). *Top insets* show the waveforms of the extracellular action potentials before (*left*) and during (*right*) the photostimulation period. Black: individual waveforms; red: averages. Raster shows the time of action potentials in different trials. The photostimulation pulse is represented by the blue bar, starting at $t = 0$ and lasting 500 ms. Continuous trace shows the peristimulus time histogram of the spikes. *D–F*: extracellular single-unit recordings at C1V1 sites in *monkey A* in response to a 200-ms pulse of green light (optimal wavelength for C1V1 activation; 532 nm, 125 mW/mm$^2$). The light pulse is represented by the green bar, starting at $t = 0$ and lasting 200 ms. All other conventions as in *C*. Photostimulation excited the units in *D* and *E* and suppressed the unit in *F*.

shows a transparent rigid-plastic stabilizer, over the AD, that has a hole to permit the passage of the fine microelectrode through the AD and into the brain. The electrode and optical fiber were independently positioned using two separate microdrives. Using the vasculature and fluorescence as references, the electrode was targeted to the ChR2 cluster and advanced under microscope guidance (Fig. 6*A*). We were able to see dimpling of the AD and of the brain and hence to identify exactly when the electrode penetrated the cortex; this was typically confirmed by the sound of neuronal activity on the audio monitor. Figure 6*B* shows a similar setup in *monkey A*.

Figure 6, *C–F*, shows examples of single-unit recordings from *monkeys C* and *A*. Figure 6*C* shows data collected from a neuron in the ChR2 cluster of *monkey C*. This unit was recorded ~0.9 mm below the cortical surface. It exhibited very low spontaneous activity (see waveforms, raster, and histogram for $t < 0$) and was clearly activated by blue light directed at the surface of the cortex (blue LED, continuous 0.5-s pulse starting at $t = 0$ s, 30 mW/mm$^2$ measured at the tip of the 2-mm diameter fiber). The spike waveforms before and during the photostimulation period are shown in the *top insets* of Fig. 6, *C–F*; waveforms collected in both periods are similar, suggesting that the recorded spikes before and during photostimulation were from the same individual neuron. Photostimulation of *monkey C*'s ChR2 site produced a significant increase in spontaneous activity for five of eight recorded units (Wilcoxon rank-sum test, $P < 0.05$).

Notice the modest irradiance (30 mW/mm$^2$) that led to robust photo-elicited responses in the experiment described in Fig. 6*C*. Also, although the AD absorbs very little light (transmission through a 0.35-mm-thick AD was 85–95%), brain tissue at 0.9-mm depth should have reduced the irradiance of the photostimulation to ~1% of its initial value at the surface (see http://www.stanford.edu/group/dlab/cgi-bin/graph/chart.php). An amount of 0.3 mW/mm$^2$ is unlikely to have driven a photosensitive neuron strongly enough to produce the robust response observed in Fig. 6*C*. We thus infer that this response was due to either direct activation of apical dendrites of the recorded neuron, near the cortical surface, or indirect activation via photosensitive neurons near the cortical surface. About half of the neurons recorded in *monkey C*'s ChR2 site were modulated by photostimulation levels <30 mW/mm$^2$. When displacing the electrode laterally, we never observed photomodulation of neuronal activity beyond ~500 $\mu$m from the ChR2 injection cluster.

*Monkey A* was injected with both AAV5 and lentivirus, each carrying a construct for C1V1, in two separate sites in V1 (Fig. 4, *E* and *F*; Table 1 specifies the C1V1 variants used). Approximately 3 wk after the injections, we recorded from the AAV5-C1V1 site (Fig. 6*B*). Figure 6*D* shows a neuron recorded at a depth of ~1 mm, which responded to light from the optical fiber (green laser, optimal to activate C1V1; continuous pulse, 0.2-s duration, starting at $t = 0$ s, 125 mW/mm$^2$). Photostimulation at this site significantly modulated spontaneous activity for 16 of 17 recorded units (Wilcoxon rank-sum test, $P < 0.05$). Figure 6, *E* and *F*, shows examples recorded from the Lenti-C1V1 site. The neuron in Fig. 6*E* was activated by photostimulation and shows a quiescent postactivation period (see raster; $0.2 < t < 0.4$ s). The unit in Fig. 6*F* was suppressed during photostimulation, an effect seen in ~20% of the neurons significantly modulated at the Lenti-C1V1 site (Fig. 7). Since lentivirus-expressing protein under the CaMKII$\alpha$ promoter selectively targets pyramidal neurons (Han et al. 2009), this suppression resulted, presumably, from the action of inhibitory neurons activated indirectly by optogenetically stimulated excitatory neurons (Han et al. 2009). We recorded from a sufficiently large sample of neurons at this site to perform population analysis, finding that 89 of 138 units were significantly modulated with light stimulation of 125 mW/mm$^2$ irradiance (Wilcoxon rank-sum test, $P < 0.05$; Fig. 7). Together, the population of recorded units had a mean modulation magnitude (stimulation rate minus baseline rate) of 30.8 spikes per second (Fig. 7).

In sum, reliable photomodulation of neuronal activity was obtained by focal illumination at the cortical surface. Electrophysiological recordings were obtained over months, without cortical damage.

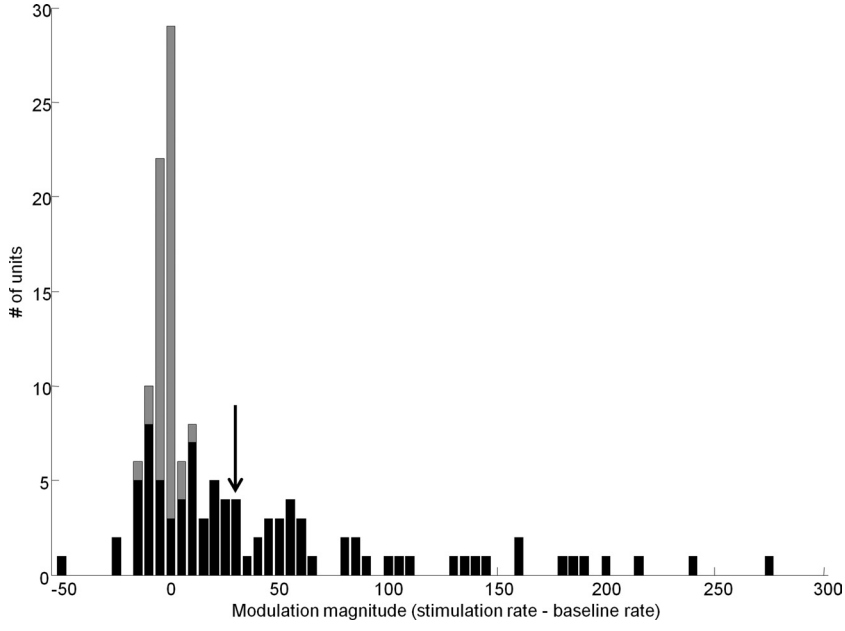


Fig. 7. Photomodulation effects across the V1 neuronal population in *monkey A*. Frequency histogram indicates number of units as a function of modulation magnitude (stimulation rate minus baseline rate; spikes per second) for the entire population recorded at the Lenti-CaMKII$\alpha$-C1V1 injection site in *monkey A*. Eighty-nine of one hundred and thirty-eight units were significantly modulated with light stimulation of 125 mW/mm$^2$ irradiance (Wilcoxon rank-sum test, $P < 0.05$). Units significantly modulated by light stimulation are indicated by black-filled bars. Together, the population of recorded units had a mean modulation magnitude of 30.8 spikes per second (indicated by black arrow).

## DISCUSSION

### *Challenges for Conducting Optogenetics in the NHP*

To date, a handful of studies have used optogenetics as a tool to modulate neuronal activity in the NHP (Cavanaugh et al. 2012; Diester et al. 2011; Galvan et al. 2012; Gerits et al. 2012; Han et al. 2009, 2011; Jazayeri et al. 2012). These studies have demonstrated proof of principle but also highlighted several shortcomings of this approach. Two key issues make the application of optogenetics in NHPs more difficult than in other model systems: *1*) the thickness and opacity of the primate dura mater; and *2*) the need to affect large volumes and numbers of neurons given the large brain of primates without causing damage to the tissue. To overcome these challenges, we aimed to achieve the following.

*Minimize cortical damage.* Unlike the dura mater of rodents, NHP dura mater is tough and cannot be penetrated by fine glass micropipettes to inject optogenetic viral vectors. Instead, injections are typically made with cannulae having diameters of ~150 $\mu$m, which damage the cortex. Optical fibers are inserted through the native dura into the brain, sometimes inside a metal cannula or glued to electrodes (optrodes). The fiber produces damage to all neurons in its trajectory, including potentially the targeted photosensitive neurons themselves. Repeated insertion of cannulae and optrodes only compound the damage. We aimed to achieve photomodulation without tissue penetration.

*Achieve visually guided, precise targeting.* A key concern in previous studies is that electrodes and fiber optics can easily miss the opsin-expressing neurons, a problem particularly relevant for lentivirus vectors, which has limited spread in the cortex (Dittgen et al. 2004; Nathanson et al. 2009). The use of a chamber-mounted grid is not sufficient to guarantee repeatability because cortex can shift up to millimeters under a cranial well (Fig. 8).

*Photostimulating larger tissue volumes.* Previous NHP studies have only achieved modest behavioral effects (Cavanaugh et al. 2012; Gerits et al. 2012); this may be due to the small volume of tissue illuminated by optrodes inserted into cortex. Given the large size of NHP brains, photostimulating a larger volume of tissue may be needed to impact behavior reliably.

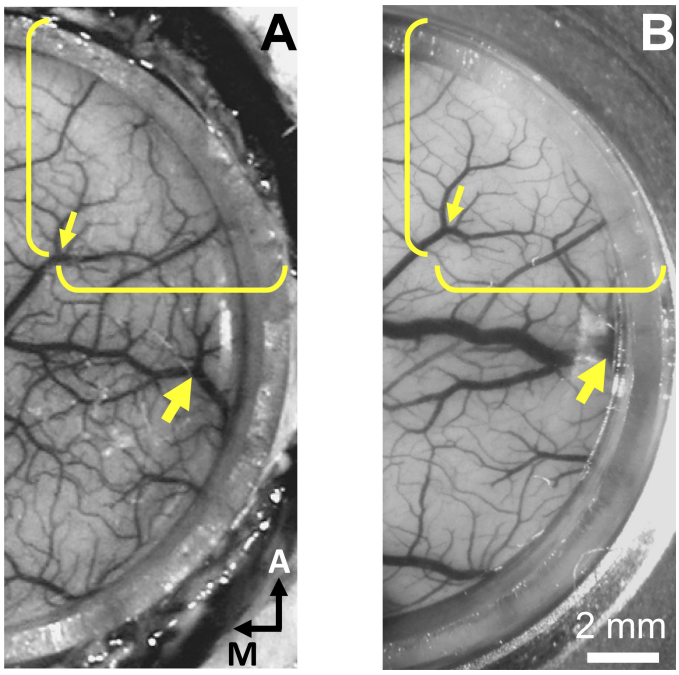


Fig. 8. Example of brain cortex shift under a cranial well. *A*: photograph of *monkey C*'s V1 immediately after implantation of an AD and cranial well. Photograph was taken while the monkey was on the operating table with his head in a stereotaxic frame. *B*: same view of *monkey C*'s chamber, 40 days later, when the monkey was seated in his chair during a behavioral experiment. The exposed brain is displaced anterolaterally. Yellow brackets and small arrow in *A* point to a conspicuous vessel bifurcation, and the other ends of the brackets were placed on the border of the implant; the brackets are in the same position, in both photographs, relative to the chamber. The big arrow points to a 2nd vessel bifurcation; both arrows point to the same respective bifurcations in either photograph. Notice how the vessel bifurcation indicated by the small arrow shifted anterolaterally relative to the brackets (~1 mm) and how the vessel indicated by the large arrow moved closer to the border of the implant and under the wall of the AD. Shifts of similar magnitudes have been observed in other monkeys, used for optical imaging, in different sessions. We attribute these cortical shifts to mechanical repositioning of the brain following differences in the relative head-neck-thorax positioning and, possibly, to changes in brain volume. Note that, if injections and subsequent optical-fiber positioning are done blindly (using an *x-y* manipulator or guide tubes through a chamber-mounted grid), electrodes and optical fibers would miss the virus-injected locations.

### *Optogenetics in the NHP is Aided by Optical Window*

The present study introduced a new approach to primate optogenetics and showed the advantages of the optical window.

*Tissue health.* The AD permits easy, repeated, and targeted introduction of micropipettes for injection of viruses without damage to the cortex. The use of fine glass pipettes to make viral-vector injections reduces tissue damage and likely promotes better uptake and expression (Nielsen et al. 2012; Osten et al. 2007). The ability to avoid major vasculature actively is also an advantage that cannot be overemphasized. Our use of non-tissue-penetrating optical fibers eliminates cortical damage during photostimulation. Less tissue damage presumably results in more cells that can express virus and hence more effective photostimulation of neuronal circuitry as well as better assessment of neuronal responses (Gerits et al. 2012; Gerits and Vanduffel 2013).

*Monitoring expression in vivo.* Typically, optogenetic expression takes several weeks. During this time, there is uncertainty about whether the virus has expressed and whether additional injections might be called for. We provide evidence that with the optical window it is possible to monitor viral expression in vivo by means of noninvasive epifluorescence imaging (Figs. 4 and 9). The ability to do so will likely depend on several factors not studied systematically here, including the number and density of neurons infected by the virus, the level of fluorescent reporter gene expression, and the depth of expression relative to the cortical surface.

*Accurate targeting.* The AD offers the ability to visualize accurately and repeatedly the desired injection, electrode, or light-fiber locations. Injections of different viruses at different locations can easily be accommodated and photostimulation effects more readily interpreted without ambiguity. Accurate targeting of microelectrodes is also critical for interpreting the effect of photostimulation on the underlying neuronal circuitry.

*Large field of view.* Most previous optogenetic studies in monkeys have relied on electrophysiological single-unit recordings to assess photostimulation effects. Combining optogenetics with optical imaging provides the ability to examine

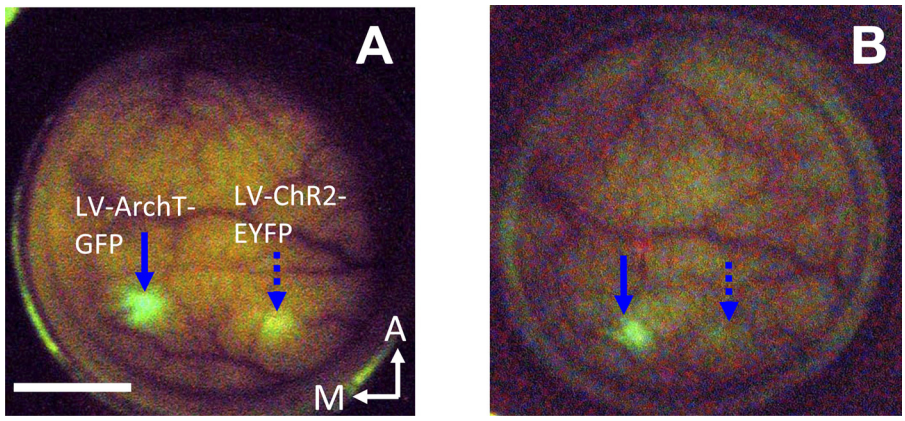


Fig. 9. In vivo epifluorescence time course: preliminary observations. *A*: epifluorescence image of *monkey C*'s chamber 7 days after Lenti-CaMKIIα-ArchT-GFP injections (blue arrow) and 23 days after Lenti-CaMKIIα-ChR2-EYFP injections (dotted blue arrow); blue-excitation/green-emission filters (reproduced from Fig. 4*D*). Scale bar: 5 mm. *B*: same view and optical setup as *A* 3 mo later (the brain surface looks slightly different in the 2 photographs because of differences in camera angle). Arrows in *B* were placed in the same positions relative to the vasculature as in *A*. Fluorescence can be observed at the same sites within the implant in *A* and *B*. The fluorescence in the later photograph (*B*) is somewhat dimmer, and the fluorescence intensity maxima are shifted slightly relative to their earlier locations (as confirmed from a detailed analysis in relation to nearby vessels). The change of surface fluorescence geometry may indicate that optogenetic expression is dynamic and continues to develop over time. We observed that the neomembrane that grows between the cortex and AD contributes to a diminished fluorescence intensity over time. Further studies combining in vivo surface epifluorescence imaging, optogenetics, and postmortem histology should provide a more detailed characterization of the in vivo surface fluorescence signals reported here.

the response of large neuronal populations across a cortical expanse. Optical modulation of known functional networks (e.g., ocular dominance, orientation, color, or motion-processing networks) as well as global networks across cortical areas opens the door to many studies of intra- and interareal cortical neuronal circuitry.

*Long-term viability.* Our study indicates that viral injections, protein expression, nor the replacement of the native dura mater with an AD was deleterious to the health or function of the cortex. The long-term (months to years) health and viability of this preparation makes it amenable for use in behavioral studies in awake, behaving monkeys (Lu et al. 2010; Tanigawa et al. 2010).

### *Limitations of the AD Approach*

*Maintenance and potential for infection.* We maintain aseptic conditions surrounding the implant during cleaning and place gauze with antibiotic on top of the AD before closing the chamber. We think that these two factors are critical for the long-term health of the implant. However, we have not performed systematic tests to compare susceptibility to infection in AD and conventional chambers (see also Arieli et al. 2002). Several months postimplantation, it is necessary to remove the neomembrane that slowly grows over the cortex and eventually becomes opaque. Removal of this neomembrane requires more care than a standard durotomy as there is typically fine connective tissue between the cortex and neomembrane.

*Target depth.* Most of the advantages conferred by the AD approach described here are limited to target structures near the surface of the brain. In particular, regions of cortex not buried within sulci are most amenable, as long as placing a recording chamber is not hampered by the presence of critical muscles over the skull. For deeper structures, it is unlikely that viral expression could be monitored noninvasively with standard epifluorescence imaging techniques and equally unlikely that light stimulation from above the AD could reach its target with enough intensity to activate optogenetic channels. Two-photon imaging and optogenetic stimulation may extend the range of target depths (Oron et al. 2012; Prakash et al. 2012) as would newly developed opsins sensitive to significantly longer wavelengths of light (Sineshchekov et al. 2012). Furthermore, the AD does not preclude one from using optical probes and other optogenetic devices that can deliver light and record electrophysiological activity directly in deeper structures.

In conclusion, the optical window permits the combination of optogenetics with traditional methods, such as electrophysiology and optical imaging, in both anesthetized and awake, behaving NHPs. Coupled with imaging methods (optical imaging or fMRI) in the awake, behaving monkey, our approach holds great promise for studying the effects of targeted cell type-specific modulation on behavior and, at the same time, mapping the underlying circuitry.

## ACKNOWLEDGMENTS

We are grateful to Dinh Diep, Aaron Cortez, Anita Disney, and Katie Williams (Salk Institute) and to Reuben Fan and Jonathan Cayce (Vanderbilt University) for experimental assistance.

## GRANTS

This work was funded by National Eye Institute (NEI) Grants R21-EY-022853 (G. R. Stoner and A. W. Roe) and R01-EY-021827 (J. H. Reynolds), Gatsby Charitable Foundation and NEI Grant R21-EY-020673 (J. J. Nassi, J. H. Reynolds, and E. M. Callaway), National Institute of Neurological Disorders and Stroke Grant NS-044375 (A. W. Roe), and shared research resources supported by NEI Core Grant for Vision Research to Vanderbilt University (P30-EY-008126) and the Salk Institute (P30-EY-019005) and the Salk Institute Innovation Grant (G. R. Stoner, T. D. Albright, and E. M. Callaway).

## DISCLOSURES

No conflicts of interest, financial or otherwise, are declared by the author(s).

## AUTHOR CONTRIBUTIONS

O.R., B.R.L., J.J.N., J.H.R., T.D.A., E.M.C., G.R.S., and A.W.R. conception and design of research; O.R., B.R.L., J.J.N., A.H.C., and A.W.R. performed experiments; O.R., B.R.L., and J.J.N. analyzed data; O.R., B.R.L.,

J.J.N., J.H.R., E.M.C., G.R.S., and A.W.R. interpreted results of experiments; O.R., B.R.L., J.J.N., and A.W.R. prepared figures; O.R., B.R.L., J.H.R., and A.W.R. drafted manuscript; O.R., B.R.L., J.J.N., J.H.R., T.D.A., E.M.C., G.R.S., and A.W.R. edited and revised manuscript; O.R., J.J.N., G.R.S., and A.W.R. approved final version of manuscript.

## REFERENCES

**Arieli A, Grinvald A, Slovin H.** Dural substitute for long-term imaging of cortical activity in behaving monkeys and its clinical implications. *J Neurosci Methods* 114: 119–133, 2002.

**Bernstein JG, Boyden ES.** Optogenetic tools for analyzing the neural circuits of behavior. *Trends Cogn Sci* 15: 592–600, 2011.

**Boyden ES, Zhang F, Bamberg E, Nagel G, Deisseroth K.** Millisecond-timescale, genetically targeted optical control of neural activity. *Nat Neurosci* 8: 1263–1268, 2005.

**Cavanaugh J, Monosov IE, McAlonan K, Berman R, Smith MK, Cao V, Wang KH, Boyden ES, Wurtz RH.** Optogenetic inactivation modifies monkey visuomotor behavior. *Neuron* 76: 901–907, 2012.

**Cayce JM, Friedman RM, Jansen ED, Mahavaden-Jansen A, Roe AW.** Pulsed infrared light alters neural activity in rat somatosensory cortex in vivo. *Neuroimage* 57: 155–166, 2011.

**Chen G, Lu HD, Roe AW.** A map for horizontal disparity in monkey V2. *Neuron* 58: 442–450, 2008.

**Chen LM, Friedman RM, Roe AW.** Optical imaging of SI topography in anesthetized and awake squirrel monkeys. *J Neurosci* 25: 7648–7659, 2005.

**Chen LM, Heider B, Williams GV, Healy FL, Ramsden BM, Roe AW.** A chamber and artificial dura method for long-term optical imaging in the monkey. *J Neurosci Methods* 113: 41–49, 2002.

**Chow BY, Han X, Dobry AS, Qian X, Chuong AS, Li M, Henninger MA, Belfort GM, Lin Y, Monahan PE, Boyden ES.** High-performance genetically targetable optical neural silencing by light-driven proton pumps. *Nature* 463: 98–102, 2010.

**Christie IN, Wells JA, Southern P, Marina N, Kasparov S, Gourine AV, Lythgoe MF.** fMRI response to blue light delivery in the naive brain: implications for combined optogenetic fMRI studies. *Neuroimage* 66C: 634–641, 2012.

**Ciocchi S, Herry C, Grenier F, Wolff SB, Letzkus JJ, Vlachos I, Ehrlich I, Sprengel R, Deisseroth K, Stadler MB, Muller C, Luthi A.** Encoding of conditioned fear in central amygdala inhibitory circuits. *Nature* 468: 277–282, 2010.

**Diester I, Kaufman MT, Mogri M, Pashaie R, Goo W, Yizhar O, Ramakrishnan C, Deisseroth K, Shenoy KV.** An optogenetic toolbox designed for primates. *Nat Neurosci* 14: 387–397, 2011.

**Dittgen T, Nimmerjahn A, Komai S, Licznerski P, Waters J, Margrie TW, Helmchen F, Denk W, Brecht M, Osten P.** Lentivirus-based genetic manipulations of cortical neurons and their optical and electrophysiological monitoring in vivo. *Proc Natl Acad Sci USA* 101: 18206–18211, 2004.

**Fenno L, Yizhar O, Deisseroth K.** The development and application of optogenetics. *Annu Rev Neurosci* 34: 389–412, 2011.

**Galvan A, Hu X, Smith Y, Wichmann T.** In vivo optogenetic control of striatal and thalamic neurons in non-human primates. *PLoS One* 7: e50808, 2012.

**Gerits A, Farivar R, Rosen BR, Wald LL, Boyden ES, Vanduffel W.** Optogenetically induced behavioral and functional network changes in primates. *Curr Biol* 22: 1722–1726, 2012.

**Gerits A, Vanduffel W.** Optogenetics in primates: a shining future? *Trends Genet* 29: 403–411, 2013.

**Gradinaru V, Mogri M, Thompson KR, Henderson JM, Deisseroth K.** Optical deconstruction of parkinsonian neural circuitry. *Science* 324: 354–359, 2009.

**Grinvald A, Frostig RD, Siegel RM, Bartfeld E.** High-resolution optical imaging of functional brain architecture in the awake monkey. *Proc Natl Acad Sci USA* 88: 11559–11563, 1991.

**Grinvald A, Lieke E, Frostig RD, Gilbert CD, Wiesel TN.** Functional architecture of cortex revealed by optical imaging of intrinsic signals. *Nature* 324: 361–364, 1986.

**Han X, Boyden ES.** Multiple-color optical activation, silencing, and desynchronization of neural activity, with single-spike temporal resolution. *PLoS One* 2: e299, 2007.

**Han X, Chow BY, Zhou H, Klapoetke NC, Chuong A, Rajimehr R, Yang A, Baratta MV, Winkle J, Desimone R, Boyden ES.** A high-light sensitivity optical neural silencer: development and application to optogenetic control of non-human primate cortex. *Front Syst Neurosci* 5: 18, 2011.

**Han X, Qian X, Bernstein JG, Zhou HH, Franzesi GT, Stern P, Bronson RT, Graybiel AM, Desimone R, Boyden ES.** Millisecond-timescale optical control of neural dynamics in the nonhuman primate brain. *Neuron* 62: 191–198, 2009.

**Huber D, Petreanu L, Ghitani N, Ranade S, Hromadka T, Mainen Z, Svoboda K.** Sparse optical microstimulation in barrel cortex drives learned behaviour in freely moving mice. *Nature* 451: 61–64, 2008.

**Jazayeri M, Lindbloom-Brown Z, Horwitz GD.** Saccadic eye movements evoked by optogenetic activation of primate V1. *Nat Neurosci* 15: 1368–1370, 2012.

**Kravitz AV, Freeze BS, Parker PR, Kay K, Thwin MT, Deisseroth K, Kreitzer AC.** Regulation of parkinsonian motor behaviours by optogenetic control of basal ganglia circuitry. *Nature* 466: 622–626, 2010.

**Lu HD, Chen G, Tanigawa H, Roe AW.** A motion direction map in macaque V2. *Neuron* 68: 1002–1013, 2010.

**Nathanson JL, Yanagawa Y, Obata K, Callaway EM.** Preferential labeling of inhibitory and excitatory cortical neurons by endogenous tropism of adeno-associated virus and lentivirus vectors. *Neuroscience* 161: 441–450, 2009.

**Nielsen KJ, Callaway EM, Krauzlis RJ.** Viral vector-based reversible neuronal inactivation and behavioral manipulation in the macaque monkey. *Front Syst Neurosci* 6: 48, 2012.

**Oron D, Papagiakoumou E, Anselmi F, Emiliani V.** Two-photon optogenetics. *Prog Brain Res* 196: 119–143, 2012.

**Osten P, Grinevich V, Cetin A.** Viral vectors: a wide range of choices and high levels of service. *Hand Exp Pharmacol* 178: 177–202, 2007.

**Prakash R, Yizhar O, Grewe B, Ramakrishnan C, Wang N, Goshen I, Packer AM, Peterka DS, Yuste R, Schnitzer MJ, Deisseroth K.** Two-photon optogenetic toolbox for fast inhibition, excitation and bistable modulation. *Nat Methods* 9: 1171–1179, 2012.

**Sineshchekov OA, Govorunova EG, Wang J, Spudich JL.** Enhancement of the long-wavelength sensitivity of optogenetic microbial rhodopsins by 3,4-dehydroretinal. *Biochemistry* 51: 4499–4506, 2012.

**Tanigawa H, Lu HD, Roe AW.** Functional organization for color and orientation in macaque V4. *Nat Neurosci* 13: 1542–1548, 2010.

**Tye KM, Prakash R, Kim SY, Fenno LE, Grosenick L, Zarabi H, Thompson KR, Gradinaru V, Ramakrishnan C, Deisseroth K.** Amygdala circuitry mediating reversible and bidirectional control of anxiety. *Nature* 471: 358–362, 2011.